

Kramers Pairs of Majorana Fermions and Parafermions in Fractional Topological Insulators

Jelena Klinovaja,¹ Amir Yacoby,¹ and Daniel Loss²

¹*Department of Physics, Harvard University, Cambridge, Massachusetts 02138, USA*

²*Department of Physics, University of Basel, Klingelbergstrasse 82, CH-4056 Basel, Switzerland*

(Dated: March 18, 2014)

We propose a scheme based on topological insulators to generate Kramers pairs of Majorana fermions or parafermions in the complete absence of magnetic fields. Our setup consists of two topological insulators whose edge states are brought close to an s -wave superconductor. The resulting proximity effect leads to an interplay between a non-local crossed Andreev pairing, which is dominant in the strong electron-electron interaction regime, and usual superconducting pairing, which is dominant at large separation between the two topological insulator edges. As a result, there are zero-energy bound states localized at interfaces between spatial regions dominated by the two different types of pairing. Due to the preserved time-reversal symmetry, the bound states come in Kramers pairs. If the topological insulators carry fractional edge states, the zero-energy bound states are parafermions, otherwise, they are Majorana fermions.

PACS numbers: 71.10.Pm; 74.45.+c; 05.30.Pr

I. INTRODUCTION

During the last decade we have witnessed a rapidly growing interest in quantum states in lower dimensions with non-trivial braiding statistics. In particular bound states at zero-energy have attracted a lot of attention. For instance, a plethora of new setups that can host Majorana fermions (MFs), particles that are their own antiparticles, has been suggested^{1–19} and motivated many experiments to test these predictions.^{20–26} These exotic particles are interesting not only from a fundamental point of view but also find a direct application in topological quantum computing schemes.²⁷ Majorana fermions are non-Abelian anyons with a braiding statistics of the Ising-type. Such anyons allow to implement some of fundamental quantum operations but not all of them.²⁸ To extend the class of operations, one can work with parafermions (PFs) that possess even more exotic braiding statistics arising in the presence of strong electron-electron interactions.^{29–40} So far, the search for most experimentally feasible setups continues as well as a discussion on which path to follow. On one hand, one can generate MFs and try to supplement their braiding statistics with non-topological gates. On the other hand, one can aim at generating non-Abelian braiding statistics of the Fibonacci type from a sea of parafermions.³⁷

In the present work we focus on Kramers pairs of Majorana fermions^{40–50} and parafermions.⁴⁰ The basic ingredients of our setup are two topological insulators^{51–64} brought into proximity to a superconductor. We assume that the chemical potential lies in the topological gap, so we focus only on edge modes, signatures of which were recently observed in experiments.^{59–64} We also note that the proximity coupling between superconductors and topological insulators were also successfully implemented.⁶⁴ Schemes for Majorana fermions in topological insulators with proximity effect have been

first proposed by Fu and Kane² and implemented in recent experiments^{20,25}, where a finite magnetic field was crucial. However, considering that magnetic fields have detrimental effects on both topological insulators and superconductors, we are motivated to keep time-reversal invariance in the system and to avoid magnetic fields altogether. This requires a different approach where the competition between Zeeman gap and superconducting proximity gap is replaced by a different mechanism, as we outline next.

The proximity to an s -wave superconductor induces superconducting pairings between edge modes that have opposite momenta and spins. Importantly for us, there are two competing superconducting mechanisms. The first one is the usual pairing that corresponds to a process where a Cooper pair tunnels as a whole in one of topological insulators. This process induces a coupling between right and left movers that also have opposite spins as a consequence of time-reversal invariance.⁵¹ The second mechanism is based on a non-local or ‘crossed Andreev’ pairing^{65–73} and corresponds to the case when a Cooper pair gets split between two topological insulators: One electron from the Cooper pair tunnels into one of the topological insulators, while its partner tunnels into the other one.

The crossed Andreev pairing dominates over the usual one in the regime of strong electron-electron interactions if the separation between edge states of neighboring topological insulators does not exceed the coherence length and the Fermi wavelength of the superconductor.⁶⁷ If the edges are separated by a large distance, the crossed Andreev pairing gets suppressed, and the usual one dominates. All this allows us to create interfaces between two different types of induced superconductivity where the two gap mechanisms compete. In such a case, one can expect the emergence of zero-energy bound states.

Indeed, we demonstrate that the crossed Andreev and usual pairing also compete with each other in the opening

of gaps in the energy spectrum. Importantly, if all pairings are of the same strength, the system is gapless. This signals the existence of two topologically distinct phases. As a consequence, there are zero-energy bound states at the interfaces between regions dominated either by the crossed Andreev or by the usual pairing. Due to the preserved time-reversal symmetry, these bound states are Kramers pairs of Majorana fermions for standard topological insulators, while they are pairs of parafermions for fractional topological insulators which carry edge states that obey fractional statistics.⁷⁴

We consider two setups that both are based on the competition between local and non-local pairing mechanisms. However, they differ by the direction of edge mode propagation in each topological insulator (or equivalently by the directions of spin orbit vectors). In our first, *para-helical*, setup considered in Sec. II, edge modes with the same spins propagate in the same direction along their common boundary in both topological insulators. In contrast to that, in our second, *ortho-helical*, setup considered in Sec. III, edge modes with opposite spins propagate in the same direction along their common boundary. In spite of this difference, our main result on the presence of zero-energy bound states with non-Abelian statistics holds for both setups.

II. PARA-HELICAL SETUP

A. Model Hamiltonian

The first setup we consider consists of two two-dimensional topological insulators (TIs),^{51–56} labeled by $\tau = 1$ and $\tau = \bar{1} (\equiv -1)$, that are brought into proximity to an s -wave superconductor, see Fig. 1. The chemical potentials μ_τ , are assumed to be equal, $\mu_1 = \mu_{\bar{1}}$, and tuned inside the band gaps of the topological insulators. The topologically protected edge modes propagate along the edges of the system in the direction determined by the spin orbit interaction (SOI) vector. In this section, we consider systems in which modes with the same spin direction propagate in the same direction along their common boundary. This can be achieved by placing two identical TIs on top of each other separated by a thin insulating layer, see Fig. 2. Alternatively, we can consider schemes involving samples with opposite signs of spin orbit interaction in the two TIs [for example, 1) by growing two samples with reversed order of layers in the heterostructure, 2) by flipping one of two identically grown samples], see Fig. 1. Thus, edge modes with spin up propagate, say, in the clockwise (anticlockwise) direction in the upper (lower) system $\tau = 1$ ($\tau = \bar{1}$), where we choose the spin quantization axis to be along the z axis perpendicular to the plane of the 2D system, see Fig. 1. As a consequence, both spin-up (down) modes propagate to the right (left) along their common boundaries. Further, we refer to this setup as the *para-helical* one (since the spin orbit vectors are opposite to each other).

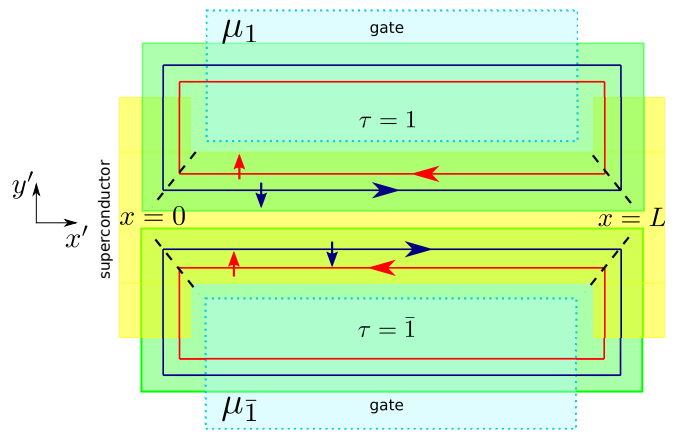


FIG. 1. Para-helical setup. Sketch of two topological insulators (green rectangles, labeled by $\tau = 1, \bar{1}$) that are tunnel-coupled to an underlying s -wave superconductor (yellow) which induces superconducting proximity effects in the TIs. The chemical potentials, controlled by the gates (light blue), are *the same* in the two samples, $\mu_1 = \mu_{\bar{1}}$. The helical edge modes (blue and red lines with arrows) in the TIs circulate in *opposite* directions due to opposite spin orbit interaction vectors. The crossed Andreev pairing dominates over the usual pairing along the common boundary of the two TIs (along the x' direction). In contrast to that, along the y' direction the dominant pairing is the usual one produced by Cooper pairs tunneling into each of the TIs as a whole. The propagation direction of spin-downs defines the x axis. The interfaces between two such regions at $x = 0$ and at $x = L$ (shown by dashed lines) host the zero-energy bound states such as Kramers pairs of Majorana fermions or Kramers pairs of parafermions depending on the nature of the TI (see text).

The kinetic part of the Hamiltonian is written as

$$H_0 = -i\hbar v_F \sum_{\tau} \int dx [R_{\tau}^{\dagger} \partial_x R_{\tau} - L_{\tau}^{\dagger} \partial_x L_{\tau}], \quad (1)$$

where v_F is the Fermi velocity. The slowly-varying right (left) mover field of the τ system $R_{\tau}(x)$ [$L_{\tau}(x)$] are defined around the Fermi points $\pm k_F$ that are determined by the position of the chemical potential μ_{τ} . Here, we choose the x axis to be always aligned with the propagation direction of the spin-down edge modes.

Next, we explore all possible proximity induced superconducting pairings taking into account that they should couple modes with opposite momenta and opposite spins.

First, Cooper pairs that tunnel together as a whole into each of the two systems lead to the usual proximity induced superconductivity of strength Δ_{τ} dependent on the tunnel coupling between the superconductor and the TIs, see Fig. 3. The corresponding pairing Hamiltonian describing this usual proximity pairing takes the form

$$H_{\tau} = \int dx \left[\frac{\Delta_{\tau}}{2} (R_{\tau}^{\dagger} L_{\tau}^{\dagger} - L_{\tau}^{\dagger} R_{\tau}^{\dagger}) + H.c. \right]. \quad (2)$$

Second, in addition to the usual proximity effect induced in each of the two systems separately, there is a

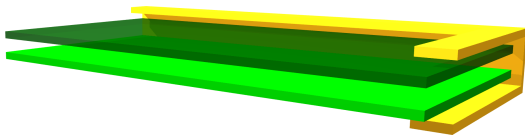


FIG. 2. Alternative realization of the para-helical setup. A bilayer consists of two identical topological insulators (dark and light green slabs) tuned at the same chemical potential. The shape of an s -wave superconductor (yellow L-shaped slab) is designed such that the crossed Andreev pairing (coupling states from different TIs) dominates along one of the edge (here, along the long edge), whereas the usual superconducting pairing (coupling states from the same TI) dominates at the other edge (here, along the short edge). Again, there are two interfaces separating the two regions, each of them containing Kramers pairs of bound states. Note that while at one interface (located at the corner of the L-shaped slab) the bound states are well-localized, there are spread out over the normal region edge states forming the other interface.

crossed (or split) Andreev process that induces a superconductivity of strength Δ_c in both systems simultaneously. Such superconducting pairing corresponds to a process when Cooper pairs get split so that one partner of the pair tunnels into one system and its partner into the other one. Consequently, such a split pairing dominates in the regime of strong electron-electron interactions since it costs less energy to insert only one electron into one edge state compared to inserting two electrons into the same edge state.^{66–68} One should also note that the crossed Andreev pairing strength Δ_c gets exponentially suppressed if the distance between the edge states of the upper and the lower TIs d exceeds the coherence length of the superconductor.^{67,71,75} Moreover, Δ_c is suppressed as an inverse power law of $(k_{Fsc}d)$, where k_{Fsc} is the Fermi wavevector of a two- or three-dimensional bulk superconductor. This suppression can be overcome, however, by using an intermediate layer of proximity induced superconductor with smaller k_{Fsc} .⁶⁹ In addition, such a spatial dependence of the crossed Andreev process enables us to envisage a third variation of the para-helical setup, see Fig. 4. This setup consists of two identical topological insulators with equal chemical potentials brought into proximity to a T-shaped superconductor. The crossed Andreev term is the strongest around $x = 0$ away from which it decays and gives way to the usual superconducting pairing at $x < -\ell_2$ and $x > \ell_1$. As a result, we again arrive at interfaces between two regions dominated by different pairing mechanisms. In what follows we focus on the setup depicted in Fig. 1 due to the simplicity of treatment of uniform pairings. However, we note that the main results, such as the presence of bound states, also hold for the non-uniform case.

The corresponding Hamiltonian for the proximity effect due to crossed Andreev superconducting pairing

takes the form

$$H_c = \int dx \left[\frac{\Delta_c}{2} (R_1^\dagger L_1^\dagger + R_1^\dagger L_1^\dagger - L_1^\dagger R_1^\dagger - L_1^\dagger R_1^\dagger) + H.c. \right], \quad (3)$$

and describes the pairing coupling between right movers with spin up from one system with left movers with spin down from the other system, see Fig. 3.

Both crossed Andreev and usual superconducting pairings open a full gap in the spectrum. As a result, one can expect a competition between two pairing mechanisms. From now on, we focus on the interfaces between two regions, see Fig. 1. In one region, the dominating superconducting pairing arises from the crossed Andreev term H_c ; in the other region, the crossed Andreev superconducting pairing is suppressed, so the edge modes are gapped only by the usual superconducting terms H_τ . Such interfaces can potentially host exotic bound states (with non-trivial braiding statistics), which is the focus of the following sections.

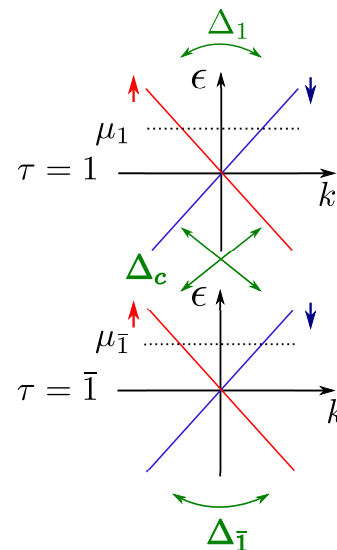


FIG. 3. The spectrum of two pairs of edge modes in topological insulators labeled by τ corresponding to the para-helical setups shown in Figs. 1 and 2. The proximity induced pairing amplitude Δ_τ induces coupling between edge modes from the same TI, resulting in proximity gaps at the Fermi level in each TI separately. If the chemical potentials μ_τ are the same in the two samples, $\mu_1 = \mu_{\bar{1}}$, the crossed Andreev pairing with amplitude Δ_c couples a spin-up state at the Fermi level in the upper TI ($\tau = 1$, red arrow) with a spin-down state at the Fermi level in the lower TI ($\tau = \bar{1}$, blue arrow), and vice versa. The crossed pairing is dominant in the regime of strong electron-electron interactions since it costs more energy to insert two charges simultaneously into the same edge of a given TI than each of them separately into different TIs.

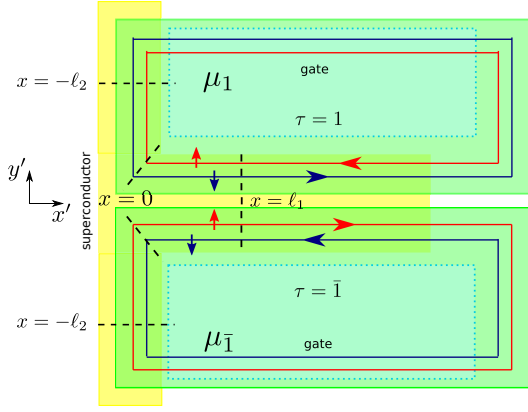


FIG. 4. Alternative realization of the para-helical setup based on a spatial decay of the crossed Andreev pairing. The setup consists of two identical topological insulators (green slabs) tuned at the same chemical potential. The shape of the s -wave superconductor (yellow T-shaped slab) is designed such that the crossed Andreev pairing (coupling states from different TIs) dominates around $x = 0$, where the distance between the samples is smallest, and decays away from this point, giving way to the usual superconducting pairing (coupling edge states from the same TI). The decay along the y' axis is determined by the coherence length and the Fermi wavelength of the superconductor. In contrast, the decay along the x' axis is much faster and arises due to a momentum mismatch between the spin-up helical edge states of one TI and the spin-down helical edge states of the other TI. As a result, there are two interfaces between different superconducting pairing regimes at $x = -\ell_2$ and $x = \ell_1$.

B. Kramers Pairs of Majorana Fermions

In this subsection, we consider an effective non-interacting single particle model of topological insulator edge modes with excitations possessing an elementary electron charge e .^{51–56} This allows us to work within the fermionic Nambu representation in the basis of eight fermion operators,^{13,76–78} $\Psi = (R_1, L_1, R_{\bar{1}}, L_{\bar{1}}, R_1^\dagger, L_1^\dagger, R_{\bar{1}}^\dagger, L_{\bar{1}}^\dagger)$. The Hamiltonian density \mathcal{H} , defined via $H = (1/2) \int dx \Psi(x)^\dagger \mathcal{H} \Psi(x)$ and the corresponding total Hamiltonian $H = H_0 + H_1 + H_{\bar{1}} + H_c$ [see Eqs. (1)-(3)], becomes written in terms of Pauli matrices,

$$\mathcal{H} = \hbar v_F \hat{k} \rho_3 - \frac{\Delta_1}{2} (1 + \tau_3) \rho_2 \eta_2 - \frac{\Delta_{\bar{1}}}{2} (1 - \tau_3) \rho_2 \eta_2 - \Delta_c \eta_2 \tau_1 \rho_2, \quad (4)$$

where $\hbar \hat{k}$ is the momentum operator. Here, the Pauli matrices ρ_i (η_i) act in left-right mover (electron-hole) space, and the Pauli matrices τ_i act in sample space. In addition, without loss of generality, we assume that Δ_τ and Δ_c are non-negative. The energy spectrum of Eq. (4)

is given by

$$E_{\pm, \pm} = \pm \left[\left(\Delta_1^2 + \Delta_{\bar{1}}^2 + 2\Delta_c^2 + 2(\hbar v_F k)^2 \right) \pm (\Delta_1 + \Delta_{\bar{1}}) \sqrt{(\Delta_1 - \Delta_{\bar{1}})^2 + 4\Delta_c^2} \right]^{1/2}, \quad (5)$$

where k is the momentum and each level $E_{\pm, \pm}$ is twofold degenerate (at fixed k), which is a direct consequence of the assumed time-reversal invariance of the system. The system gap is defined by the energy difference at $k = 0$, *i.e.*, $2|\Delta_{k=0}| \equiv E_{+, -}(k=0) - E_{-, -}(k=0)$, which gives explicitly

$$\Delta_{k=0} = \left[\Delta_1 + \Delta_{\bar{1}} - \sqrt{(\Delta_1 - \Delta_{\bar{1}})^2 + 4\Delta_c^2} \right] / 2. \quad (6)$$

From this we see immediately that the spectrum is gapless if $\Delta_c^2 = \Delta_1 \Delta_{\bar{1}}$, while it is fully gapped otherwise. The closing and reopening of the gap as a function of system parameters could signal a topological phase transition that separates two superconducting phases: the topological one with $\Delta_{k=0} < 0$ and the trivial one with $\Delta_{k=0} > 0$. If an interface between such two phases (two regions in real space) is created, it should host localized zero energy states. In the first region the gap is dominated by, say, the crossed Andreev superconductivity Δ_c with $\Delta_{k=0} < 0$. In the second region, the gap is determined by the usual pairing Δ_1 and $\Delta_{\bar{1}}$, respectively, with $\Delta_{k=0} > 0$.

As an example, we consider such an interface at $x = 0$ separating two regions characterized by different strengths of the crossed Andreev pairing amplitude: $\Delta_c > \sqrt{\Delta_1 \Delta_{\bar{1}}} > 0$ for $x > 0$ and $\Delta_c = 0$ for $x < 0$. The usual pairing amplitudes Δ_τ are assumed to be uniform for the sake of simplicity. Indeed, at this interface, we find two zero-energy bound states Ψ_{MF1} and $\Psi_{MF\bar{1}}$ localized at $x = 0$. These two states are Majorana fermions, $\hat{\Psi}_{MF i} = \hat{\Psi}_{MF i}^\dagger$, and they are Kramers partners, $\Psi_{MF1} = T \Psi_{MF\bar{1}}$. Here, $T = i\sigma_2 K$ is the time reversal operator composed of K , the complex conjugation operator [$\Psi^*(x) = K \Psi(x)$], and of the Pauli matrix σ_i acting on spin. In general, a Kramers pair of Majorana fermion wavefunctions can be written in the basis $\tilde{\Psi} = (\Psi_{1, \downarrow}, \Psi_{1, \uparrow}, \Psi_{\bar{1}, \downarrow}, \Psi_{\bar{1}, \uparrow}, \Psi_{1, \downarrow}^\dagger, \Psi_{1, \uparrow}^\dagger, \Psi_{\bar{1}, \downarrow}^\dagger, \Psi_{\bar{1}, \uparrow}^\dagger)$ as

$$\Psi_{MF1}(x) = \begin{pmatrix} f_1(x) \\ g_1(x) \\ f_{\bar{1}}(x) \\ g_{\bar{1}}(x) \\ f_1^*(x) \\ g_1^*(x) \\ f_{\bar{1}}^*(x) \\ g_{\bar{1}}^*(x) \end{pmatrix}, \quad \Psi_{MF\bar{1}}(x) = \begin{pmatrix} g_{\bar{1}}^*(x) \\ -f_{\bar{1}}^*(x) \\ g_1^*(x) \\ -f_1^*(x) \\ g_1(x) \\ -f_1(x) \\ g_{\bar{1}}(x) \\ -f_{\bar{1}}(x) \end{pmatrix}, \quad (7)$$

where the complex functions $f_\tau(x)$ and $g_\tau(x)$ are, in principle, arbitrary up to the normalization prefactor which will be suppressed in the following. The annihilation (creation) operators $\Psi_{\tau, \sigma}$ ($\Psi_{\tau, \sigma}^\dagger$) act on electrons with spin $\sigma = \uparrow, \downarrow$ located in the τ wire. We note that wavefunctions

in the basis $\tilde{\Psi}$ can be easily obtained from wavefunctions written in the basis Ψ by restoring the fast oscillating factors $e^{\pm ik_F x}$.

In the case of a sharp drop of the crossed Andreev pairing amplitude Δ_c at $x = 0$ specified above, these functions are obtained straightforwardly⁷⁷ and given by

$$\begin{aligned} f_1 &= -ig_1^* = s_1 \frac{\Delta_1 - \Delta_{\bar{1}} - \sqrt{(\Delta_1 - \Delta_{\bar{1}})^2 + 4\Delta_c^2}}{2\Delta_c}, \\ f_{\bar{1}} &= -ig_{\bar{1}}^* = s_{\bar{1}}, \\ s_\tau &= e^{-ik_F x} \times \begin{cases} e^{-x/\xi_c}, & x > 0 \\ -e^{x/\xi_\tau}, & x < 0. \end{cases} \end{aligned} \quad (8)$$

The localization lengths ξ_c and ξ_τ are inverse proportional to the gaps opened at the Fermi points and are explicitly given by

$$\begin{aligned} \xi_c &= 2\hbar v_F / (\sqrt{(\Delta_1 - \Delta_{\bar{1}})^2 + 4\Delta_c^2} - \Delta_1 - \Delta_{\bar{1}}), \\ \xi_\tau &= \hbar v_F / \Delta_\tau. \end{aligned} \quad (9)$$

Above we have considered only the interface at $x = 0$. An analogous interface also occurs at the other end, $x = L$, of the region dominated by crossed Andreev pairing (see Fig. 1). By analogy, we can show that it hosts also a Kramers pair of Majorana fermions. If the length of the crossed Andreev dominated region is much longer than the localization length, $L \gg \xi \equiv \max\{1/\xi_c, 1/\xi_\tau\}$, the wavefunctions of the MFs localized at two different interfaces do not overlap, so the MFs can be considered as independent. If L gets comparable with the localization length ξ , two overlapping MFs hybridize into a complex fermionic state whose energy is generally non-zero.⁷⁹ We note that the two MFs of the same Kramers pair are located at the same position but being orthogonal states do not hybridize as long as time-reversal symmetry is present.⁴⁰⁻⁵⁰ If this symmetry is broken, e.g. by an external magnetic field or by magnetic impurities, then they can also split in energy away from zero and become a complex fermionic state.

C. Kramers Pairs of Parafermions in Fractional Topological Insulators

So far we have worked with an effective single particle Hamiltonian, which is appropriate in the regime considered. In this subsection, we focus on the regime where electron-electron interactions dominate and work with fractional topological insulators in which elementary excitations possess an effective charge e/m with m being a positive odd integer.^{74,80}

To analyze this problem we make use of the bosonization formalism. In terms of chiral bosonic fields $\phi_{r\tau}$, the electron operators are then rewritten as $R_\tau = e^{im\phi_{1\tau}}$ and $L_\tau = e^{im\phi_{\bar{1}\tau}}$. By analogy, we introduce chiral bosonic fields $\tilde{\phi}_{r\tau}$ describing hole operators in Nambu space. To satisfy the anticommutation relations between original

fermionic operators, we work with the following non-zero commutators for the bosonic fields,

$$[\phi_{r\tau}(x), \phi_{r'\tau'}(x')] = \frac{i\pi r}{m} \delta_{rr'} \delta_{\tau\tau'} \text{sgn}(x - x'), \quad (11)$$

$$[\tilde{\phi}_{r\tau}(x), \tilde{\phi}_{r'\tau'}(x')] = \frac{i\pi r}{m} \delta_{rr'} \delta_{\tau\tau'} \text{sgn}(x - x'). \quad (12)$$

All other commutators are assumed to vanish.

To proceed, we bosonize the Hamiltonians H_τ [see Eq. (2)] and H_c [see Eq. (3)],

$$\begin{aligned} H_c &= \Delta_c (\cos[m(\phi_{11} - \tilde{\phi}_{\bar{1}\bar{1}})] + \cos[m(\phi_{\bar{1}\bar{1}} - \tilde{\phi}_{11}]) \\ &\quad - \cos[m(\phi_{\bar{1}\bar{1}} - \tilde{\phi}_{11})] - \cos[m(\phi_{11} - \tilde{\phi}_{\bar{1}\bar{1}})]), \end{aligned} \quad (13)$$

$$H_1 = \Delta_1 (\cos[m(\phi_{11} - \tilde{\phi}_{\bar{1}\bar{1}})] - \cos[m(\phi_{\bar{1}\bar{1}} - \tilde{\phi}_{11})]), \quad (14)$$

$$H_{\bar{1}} = \Delta_{\bar{1}} (\cos[m(\phi_{\bar{1}\bar{1}} - \tilde{\phi}_{11})] - \cos[m(\phi_{11} - \tilde{\phi}_{\bar{1}\bar{1}})]). \quad (15)$$

Furthermore, in Nambu representation one can easily see that the total Hamiltonian can be separated into two independent (commuting) parts, $H^{(1)}$ and $H^{(\bar{1})}$, so that $H = H^{(1)} + H^{(\bar{1})}$. Here, $H^{(1)}$ [$H^{(\bar{1})}$] act in the subspace composed of $\phi_{1\tau}$ and $\tilde{\phi}_{\bar{1}\tau}$ ($\phi_{\bar{1}\tau}$ and $\tilde{\phi}_{1\tau}$). These two parts are connected by time-reversal symmetry, so their eigenstates are Kramers partners of each other. The non-quadratic part of $H^{(1)}$ consists of $H_1^{(1)}$, $H_{\bar{1}}^{(1)}$, and $H_c^{(1)}$ given by

$$\begin{aligned} H_c^{(1)} &= \Delta_c (\cos[m(\phi_{11} - \tilde{\phi}_{\bar{1}\bar{1}})] \\ &\quad + \cos[m(\phi_{\bar{1}\bar{1}} - \tilde{\phi}_{11})]), \end{aligned} \quad (16)$$

$$H_1^{(1)} = \Delta_1 \cos[m(\phi_{11} - \tilde{\phi}_{\bar{1}\bar{1}})], \quad (17)$$

$$H_{\bar{1}}^{(1)} = \Delta_{\bar{1}} \cos[m(\phi_{\bar{1}\bar{1}} - \tilde{\phi}_{11})]. \quad (18)$$

From now on, we focus on $H^{(1)}$, keeping in mind that the eigenstates of $H^{(\bar{1})}$ can be easily obtained by acting with the time-reversal operator T on the eigenstates of $H^{(1)}$.

In a next step, we express the chiral fields $\phi_{1\tau}$ and $\tilde{\phi}_{\bar{1}\tau}$ in terms of the conjugated ϕ_η and θ_η fields, $\eta = \pm 1$, defined as

$$\phi_1 = m(\phi_{11} + \phi_{\bar{1}\bar{1}} - \tilde{\phi}_{\bar{1}\bar{1}} - \tilde{\phi}_{11})/2, \quad (19)$$

$$\theta_1 = m(\phi_{11} + \phi_{\bar{1}\bar{1}} + \tilde{\phi}_{\bar{1}\bar{1}} + \tilde{\phi}_{11})/2, \quad (20)$$

$$\phi_{\bar{1}} = m(\phi_{11} - \phi_{\bar{1}\bar{1}} - \tilde{\phi}_{\bar{1}\bar{1}} + \tilde{\phi}_{11})/2, \quad (21)$$

$$\theta_{\bar{1}} = m(\phi_{11} - \phi_{\bar{1}\bar{1}} + \tilde{\phi}_{\bar{1}\bar{1}} - \tilde{\phi}_{11})/2, \quad (22)$$

or inverting

$$\phi_{1\tau} = \left(\frac{\phi_1 + \theta_1}{m} + \tau\phi_{\bar{1}} + \tau\theta_{\bar{1}} \right) / 2, \quad (23)$$

$$\tilde{\phi}_{\bar{1}\tau} = \left(\frac{-\phi_1 + \theta_1}{m} - \tau\phi_{\bar{1}} + \tau\theta_{\bar{1}} \right) / 2. \quad (24)$$

As a result, $H_c^{(1)}$ and $H_\tau^{(1)}$ [see Eqs. (16)-(18)] become in the new basis

$$H_c^{(1)} = 2\Delta_c \cos(\phi_1) \cos(m\theta_{\bar{1}}), \quad (25)$$

$$H_1^{(1)} = \Delta_1 \cos(\phi_1 + m\phi_{\bar{1}}), \quad (26)$$

$$H_{\bar{1}}^{(1)} = \Delta_{\bar{1}} \cos(\phi_1 - m\phi_{\bar{1}}). \quad (27)$$

If there was only one interaction term present in the Hamiltonian, for example $H_c^{(1)}$ ($H_\tau^{(1)}$), and if it was relevant (in a renormalization group sense), then the corresponding coupling constant Δ_c (Δ_τ) would grow (under renormalization flow due to interactions) leading to a gapped spectrum. In addition, the combination of fields standing under the corresponding cosine would get pinned to a constant such that the total energy is minimized.⁸⁵

However, if both terms $H_c^{(1)}$ and $H_\tau^{(1)}$ are present, only one of them can be ordered (so that the corresponding fields get pinned), as the crossed Andreev term H_c and the usual pairing term H_τ do not commute with each other. This is easily seen from Eqs. (2) and (3) written in the fermionic representation. However, one can arrive at the same conclusion also in the bosonic representation [see Eqs. (25)-(27)] by using the commutation relations for the new fields ϕ_η and θ_η obtained from Eqs. (11) and (12):

$$\begin{aligned} [\phi_{\bar{1}}(x), \theta_{\bar{1}}(x')] &= \frac{i\pi}{m} \text{sgn}(x - x'), \\ [\phi_1(x), \theta_1(x')] &= [\phi_1(x), \phi_{\bar{1}}(x')] = 0, \end{aligned} \quad (28)$$

where, in addition, each of the bosonic fields commutes with itself. As a consequence, the two different pairing terms do not commute and thus cannot be ordered simultaneously within the same space region. To avoid this situation, in what follows we thus work in the regime of strong electron-electron interactions such that H_c dominates over H_τ if both of them are present, and pinning is possible. Interaction effects favor energetically the separation and injection of the two electrons from a Cooper pair into separate edges over a simultaneous injection of the two electrons as a whole into the same edge.

Similarly, to the effective single-particle case considered in the previous subsection, we focus on the interface separating the region dominated by crossed Andreev pairing from the regions where the usual pairing dominates, see Fig. 1. The crossed Andreev term H_c is dominant inside the interval $0 < x < L$ which is surrounded by two regions, $x < 0$ and $x > L$, where the usual superconducting terms H_τ are dominant.

Deep inside the region $0 < x < L$ [$x < 0$ or $x > L$], the corresponding bosonic fields ϕ_1 and $\theta_{\bar{1}}$ (ϕ_1 and $\phi_{\bar{1}}$) are pinned as to minimize the total energy, see Fig. 5. First, we note that the bosonic field ϕ_1 should be pinned uniformly in the entire system, $\phi_1 = \pi\hat{M}$. Second, the other fields are pinned as

$$\phi_1 = \begin{cases} \pi(\hat{M} + 1 + 2\hat{l}_{\bar{1}})/m, & x < 0, \\ \pi(\hat{M} + 1 + 2\hat{l}_1)/m, & x > L, \end{cases} \quad (29)$$

$$\theta_{\bar{1}} = \pi(\hat{M} + 1 + 2\hat{n})/m, \quad x \in (0, L). \quad (30)$$

Here, \hat{M} , \hat{n} , and \hat{l}_τ are integer-valued operators. The commutation relations between them follow from

Eqs. (28) and are given by

$$[\hat{l}_{\bar{1}}, \hat{n}] = -[\hat{l}_1, \hat{n}] = -\frac{im}{4\pi}, \quad (31)$$

$$[\hat{M}, \hat{n}] = [\hat{M}, \hat{l}_1] = [\hat{M}, \hat{l}_{\bar{1}}] = 0. \quad (32)$$

As a result of the two fields being pinned simultaneously (ϕ_1 and $\theta_{\bar{1}}$ in the crossed Andreev region; ϕ_1 and $\phi_{\bar{1}}$ in the usual pairing region), the energy spectrum away from interfaces is fully gapped. In other words, the system does not host zero-energy states in the bulk.^{35,37}

Importantly, while two non-commuting fields cannot be pinned simultaneously, at interfaces between two regions both $\phi_{\bar{1}}$ and $\theta_{\bar{1}}$ are fluctuating inside the interface region of size ℓ and the bulk gap can close (apart from finite size level spacings).³⁵ Consequently, the interfaces might host zero-energy states with the localization length determined by ℓ . To identify these states, we define the operator α_1 ($\alpha_{\bar{1}}$) at the interface $x = 0$ ($x = L$):

$$\alpha_1 = e^{i\frac{2\pi}{m}(\hat{n} + \hat{l}_1) - i\frac{\pi}{2}}, \quad \alpha_{\bar{1}} = e^{i\frac{2\pi}{m}(\hat{n} + \hat{l}_{\bar{1}}) + i\frac{\pi}{2}}, \quad (33)$$

These operators are easily seen to commute with the total Hamiltonian, and thus they represent zero-energy bound states.³⁵

Next, we identify the properties of α operators using derived above commutators between the integer-valued operators, see Eqs. (31) and (32). First, we note that $\alpha_\tau^m = 1$. Second, we obtain for the commutation relations between two different operators

$$\alpha_1 \alpha_{\bar{1}} = \alpha_{\bar{1}} \alpha_1 e^{2\pi i/m}. \quad (34)$$

These operators thus possess the same properties as \mathbb{Z}_m parafermion operators.

We also identify the degeneracy of the ground state. The operator $\alpha_1^\dagger \alpha_{\bar{1}} = -e^{-i\pi/m} e^{2\pi i(\hat{l}_{\bar{1}} - \hat{l}_1)/m}$ has the property that $(\alpha_1^\dagger \alpha_{\bar{1}})^m = 1$. Its m eigenstates denoted as $|q\rangle$ correspond to the eigenvalues $e^{2\pi i q/m}$. Thus, the ground state of $H^{(1)}$ and $H^{(\bar{1})}$ is m -fold degenerate.^{35,37} Taking into account Kramers degeneracy, we find that the

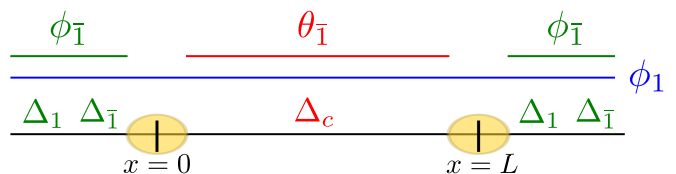


FIG. 5. Pinning of bosonic fields in the regime of strong electron-electron interactions. The field ϕ_1 (blue line) is pinned uniformly in the entire system. The field $\phi_{\bar{1}}$ ($\theta_{\bar{1}}$) is pinned in the region where the usual pairing term Δ_τ (crossed Andreev pairing term Δ_c) is dominant, indicated by green (red) lines. The different regions are separated by interfaces of size ℓ located at $x = 0$ and $x = L$ (yellow circles). Within these interfaces the non-commuting fields $\phi_{\bar{1}}$ and $\theta_{\bar{1}}$ overlap and fluctuate, giving rise to zero-energy bound states that can be identified as Kramers pairs of parafermions (one pair at each interface).

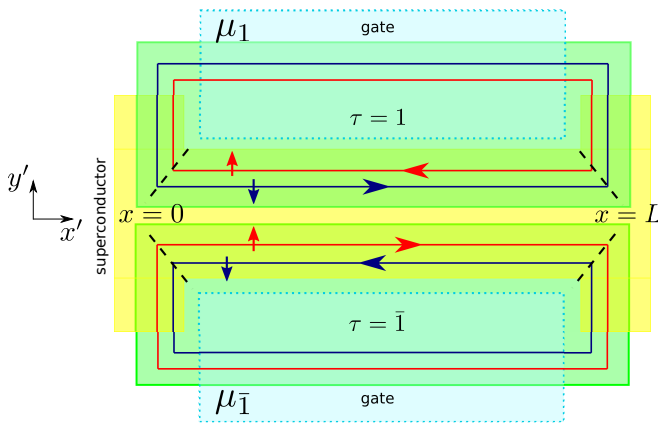


FIG. 6. Ortho-helical setup. Sketch of two topological insulators ($\tau = \pm 1$, green rectangles) brought into proximity to a superconductor (yellow). The chemical potentials, controlled by the gates (light blue), are tuned to be *opposite* in the two samples, $\mu_1 = -\mu_{\bar{1}}$. The edge modes circulate in *the same* direction in both samples as their spin orbit interaction vectors are codirectional. As a result of strong electron-electron interactions, the crossed Andreev superconducting pairing dominates over the usual superconducting pairing along the common boundary of the two samples (x' direction). In contrast to that, in the region where the edge states propagate along the y' direction, the only present superconducting pairing is the usual one produced by Cooper pairs tunneling into one of the samples as a whole.

ground state of the system described by $H = H^{(1)} + H^{(\bar{1})}$ is represented by m Kramers pairs of parafermions.

III. ORTHO-HELICAL SETUP

A. Model Hamiltonian

The model considered in this section is similar to the one considered above in Sec. II. The main ingredients are the same: the two topological insulators,^{51–56,74} again labeled by $\tau = 1, \bar{1}$, are brought into the proximity to an ordinary s -wave superconductor. However, in contrast to the previous case, the spin orbit vectors of the two TIs are both aligned in the positive direction along the z axis. This means that in both systems spin up (down) states propagate in the clockwise (anticlockwise) direction, see Fig. 6. We refer to this case as to the *ortho-helical* setup (since the spin orbit interaction vectors point along the same direction).

Alternatively, one can also aim at using pairs of edge modes localized at the opposite edges of a *single* topological insulator. However, such a setup poses some additional difficulties for implementations. First, it is challenging to keep the chemical potentials at opposite values $\mu_1 = -\mu_{\bar{1}}$ at opposite edges in the *same* sample where all edge states are connected. So, the setup should be tuned close to the Dirac point $\mu_1 \approx -\mu_{\bar{1}} \approx 0$, which, however, requires very precise control. Second, a compromise for

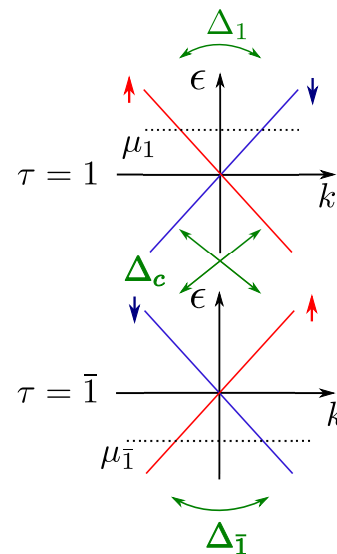


FIG. 7. The spectrum of two pairs of edge modes in topological insulators corresponding to the ortho-helical setup shown in Fig. 6. The superconducting pairing is similar to the one shown in Fig. 3, with the difference that here the chemical potentials μ_τ are opposite at the two edges, $\mu_1 = -\mu_{\bar{1}}$. In this case, the crossed Andreev pairing with amplitude Δ_c couples a spin-up state at the Fermi level in the upper TI ($\tau = 1$, blue arrow) with a spin-down state at the Fermi level in the lower TI ($\tau = \bar{1}$, red arrow), and vice versa. Again, the crossed pairing is dominant in the regime of strong electron-electron interactions.

the sample width needs to be found. On one hand, the edge modes from opposite edges separated by d should not overlap, thus d should be much larger than the penetration length of edge states inside the sample. On the other hand, the separation d should be smaller than the coherence length of the superconductor in order for the crossed Andreev pairing to be dominant. All this makes an experimental realization using a single TI presumably more challenging than using two of them.

We emphasize that for notational simplicity we use the same symbols for fermionic and bosonic operators and Hamiltonians as in the previous section. We believe that this should not lead to ambiguities, as long as we clearly distinguish between ortho-helical and para-helical setups.

As before, the kinetic part of the Hamiltonian is written in terms of slowly moving right- [$R_\tau(x)$] and left- [$L_\tau(x)$] fields defined around the Fermi points $\pm k_F$ as

$$H_0 = -i\hbar v_F \sum_\tau \int dx [R_\tau^\dagger \partial_x R_\tau - L_\tau^\dagger \partial_x L_\tau]. \quad (35)$$

Here, v_F is the Fermi velocity, and the index τ refers to the corresponding TI. Importantly, the spin up mode corresponds to the right (left) moving field in the upper (lower) sample $\tau = 1$ ($\tau = \bar{1}$), see Fig. 7. In addition, we choose here the x axis to be codirectional with the propagation direction of the spin down (spin up) mode in the $\tau = 1$ ($\tau = \bar{1}$) system.

Again, the most important ingredients of our setup are pairing terms induced by an ordinary s -wave superconductor in proximity contact to the TIs. Such terms are responsible for couplings between states with opposite momenta and spins. We note that the only way to generate a crossed Andreev term, which pairs modes from different TIs, is to tune the chemical potentials to be opposite in the two TIs, $\mu_1 = -\mu_{\bar{1}}$, see Fig. 7. The corresponding term in the Hamiltonian is written as

$$H_c = \int dx \frac{\Delta_c}{2} (R_1^\dagger R_1^\dagger - R_1^\dagger R_1^\dagger + L_1^\dagger L_1^\dagger - L_1^\dagger L_1^\dagger + H.c.), \quad (36)$$

where Δ_c is the crossed Andreev pairing amplitude. Similarly, we write down the usual pairing term with amplitude Δ_τ induced in each of the TIs separately,

$$H_t = \sum_\tau \int dx \left[\frac{\Delta_\tau}{2} (R_1^\dagger L_1^\dagger - L_1^\dagger R_1^\dagger) + \frac{\Delta_{\bar{\tau}}}{2} (L_1^\dagger R_1^\dagger - R_1^\dagger L_1^\dagger) + H.c. \right]. \quad (37)$$

For the proposed setup, the crossed Andreev term dominates only along the edge where the two samples are brought close to each other. Along the other edges, Δ_c is exponentially suppressed at the distance of the coherence length of the superconductor and/or power-law

like on the scale of the Fermi wavelength. This results in interfaces between the regions dominated by crossed Andreev pairing and the usual pairing regions similar to the ones considered in the previous section, see Fig. 6.

B. Kramers Pairs of Majorana Fermions

First we focus on the topological insulators that can be described in an effective single-particle model (i.e. in the absence of explicit interactions).^{51–56} In this case, we can explore the presence of the localized zero-energy states by direct diagonalization of the total Hamiltonian $H = H_0 + H_c + H_t$ in the fermionic representation. In the basis $\Psi = (R_1, L_1, R_{\bar{1}}, L_{\bar{1}}, R_1^\dagger, L_1^\dagger, R_{\bar{1}}^\dagger, L_{\bar{1}}^\dagger)$, the Hamiltonian density is written in terms of the Pauli matrices η_i (τ_i) acting in the electron-hole (channel) space^{13,76–78} as

$$\mathcal{H} = \hbar v_F \hat{k} \rho_3 - \frac{\Delta_1}{2} (1 + \tau_3) \rho_2 \eta_2 + \frac{\Delta_{\bar{1}}}{2} (1 - \tau_3) \rho_2 \eta_2 - \Delta_c \eta_2 \tau_2 \rho_3, \quad (38)$$

where ρ_i are the Pauli matrices acting in the left-right mover space.

The energy spectrum of \mathcal{H} is given by

$$E_{\pm, \pm} = \pm \left[\left(\Delta_1^2 + \Delta_{\bar{1}}^2 + 2\Delta_c^2 + 2(\hbar v_F k)^2 \pm \sqrt{(\Delta_1 + \Delta_{\bar{1}})^2 [(\Delta_1 - \Delta_{\bar{1}})^2 + 4\Delta_c^2] + (4\Delta_c \hbar v_F k)^2} \right) / 2 \right]^{1/2}, \quad (39)$$

where each energy level is twofold degenerate, again as a direct consequence of time-reversal invariance of the system, see Fig. 8. We note that the system is gapless in two cases: if $\Delta_1 = \Delta_{\bar{1}} < \Delta_c$ or if $\Delta_c^2 = \Delta_1 \Delta_{\bar{1}}$. We note here that the spectra of the para- and ortho-helical setups are identical at zero momentum but different at finite momentum [compare Eq. (7) with Eq. (39)]. Consequently, the gap at $k = 0$ defined via Eq. (6) is again closed if and only if $\Delta_c^2 = \Delta_1 \Delta_{\bar{1}}$. In addition to that, in the ortho-helical setup considered in this section, the gap also closes at finite momenta if $\Delta_1 = \Delta_{\bar{1}} < \Delta_c$, see Fig. 8. We recall that such finite-momentum closing of the gap does not occur in the para-helical case considered in Sec. II.

The closing of the gap as a function of the parameters Δ_c and Δ_τ might indicate the presence of a topological phase transition, which we explore further in detail.

In a next step, we consider an interface between two regions: one with finite crossed Andreev pairing term ($\Delta_c > 0$ for $x > 0$) and one without it ($\Delta_c = 0$ for $x < 0$). The usual superconducting terms are assumed to be of constant strength Δ_τ . At the interface $x = 0$, there

are two zero-energy Majorana bound states $\Psi_{MF1}(x)$ and $\Psi_{MF\bar{1}}(x)$ if $\Delta_c^2 > \Delta_1 \Delta_{\bar{1}}$ and $\Delta_1 \neq \Delta_{\bar{1}}$. These two states are time-reversal partners connected by $\Psi_{MF1}(x) = T \Psi_{MF\bar{1}}(x)$. The general form of two MF wavefunctions corresponding to a Kramers pair is written in the basis $\tilde{\Psi} = (\Psi_{1,\uparrow}, \Psi_{1,\downarrow}, \Psi_{\bar{1},\downarrow}, \Psi_{\bar{1},\uparrow}, \Psi_{1,\uparrow}^\dagger, \Psi_{1,\downarrow}^\dagger, \Psi_{\bar{1},\downarrow}^\dagger, \Psi_{\bar{1},\uparrow}^\dagger)$ as

$$\Psi_{MF1}(x) = \begin{pmatrix} f_1(x) \\ g_1(x) \\ f_{\bar{1}}(x) \\ g_{\bar{1}}(x) \\ f_1^*(x) \\ g_1^*(x) \\ f_{\bar{1}}^*(x) \\ g_{\bar{1}}^*(x) \end{pmatrix}, \quad \Psi_{MF\bar{1}}(x) = \begin{pmatrix} g_{\bar{1}}^*(x) \\ -f_{\bar{1}}^*(x) \\ -g_{\bar{1}}^*(x) \\ f_{\bar{1}}^*(x) \\ g_1(x) \\ -f_1(x) \\ -g_{\bar{1}}(x) \\ f_{\bar{1}}(x) \end{pmatrix}, \quad (40)$$

where $f_{\pm 1}$ and $g_{\pm 1}$ are four arbitrary complex functions (again, we suppress the normalization constant). As before, wavefunctions being rewritten from the basis Ψ to the basis $\tilde{\Psi}$ just acquire oscillating prefactors $e^{\pm i k_F x}$.⁷⁷

In the setup under consideration which assumes a sharp drop of the crossed Andreev pairing strength, these functions are given by

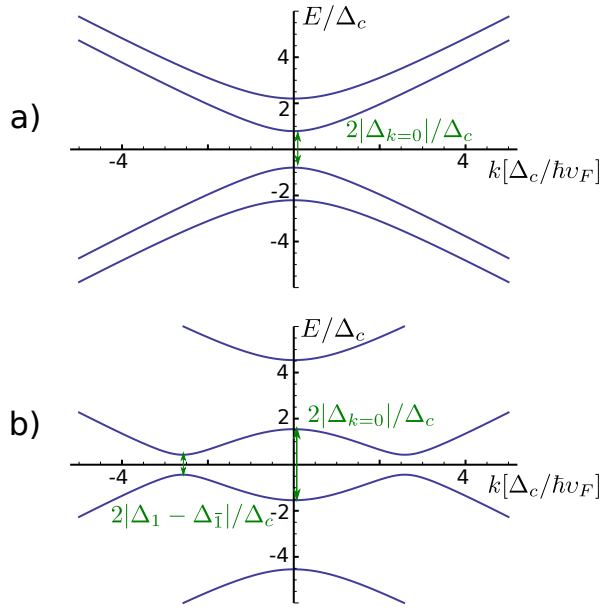


FIG. 8. The energy spectrum $E(k)$ of the system shown in Fig. 6 around the Fermi points $\pm k_F$ [see Eq. (39)]. The gap at $k = 0$ closes at $\Delta_c = \sqrt{\Delta_1 \Delta_{\bar{1}}}$, indicating the topological transition separating (a) the trivial (characterized by $\Delta_{k=0} > 0$) and (b) the topological (characterized by $\Delta_{k=0} < 0$) phases. We note that (a) in the trivial phase the gap is minimal at $k = 0$, whereas (b) in the topological phase the gap is minimal at a finite wavevector and is given by $|\Delta_1 - \Delta_{\bar{1}}|$. The parameters are chosen to be (a) $\Delta_1/\Delta_c = 4$ and $\Delta_{\bar{1}}/\Delta_c = 2$; (b) $\Delta_1/\Delta_c = 2/3$ and $\Delta_{\bar{1}}/\Delta_c = 1/3$.

$$f_1(x) = ig_1^*(x) = \begin{cases} \frac{\Delta_c i e^{ik_F x} (e^{-x/\xi_1} - e^{-x/\xi_2})}{\sqrt{(\Delta_1 + \Delta_{\bar{1}})^2 - 4\Delta_c^2}}, & x > 0 \\ 0, & x < 0 \end{cases}, \quad (41)$$

$$f_{\bar{1}}(x) = ig_{\bar{1}}^*(x) = e^{-ik_F x} \times \begin{cases} \frac{e^{-x/\xi_1} (\sqrt{(\Delta_1 + \Delta_{\bar{1}})^2 - 4\Delta_c^2} - \Delta_1 - \Delta_{\bar{1}})}{2\sqrt{(\Delta_1 + \Delta_{\bar{1}})^2 - 4\Delta_c^2}} + \frac{e^{-x/\xi_2} (\Delta_1 + \Delta_{\bar{1}} + \sqrt{(\Delta_1 + \Delta_{\bar{1}})^2 - 4\Delta_c^2})}{2\sqrt{(\Delta_1 + \Delta_{\bar{1}})^2 - 4\Delta_c^2}}, & x > 0 \\ e^{x/\xi_3}, & x < 0 \end{cases}. \quad (42)$$

Here, without loss of generality, we assume that $\Delta_1 > \Delta_{\bar{1}}$. The localization lengths $\xi_{1,2,3}$,

$$\xi_1 = 2\hbar v_F / (\Delta_1 - \Delta_{\bar{1}} + \sqrt{(\Delta_1 + \Delta_{\bar{1}})^2 - 4\Delta_c^2}), \quad (43)$$

$$\xi_2 = 2\hbar v_F / (\Delta_1 + \Delta_{\bar{1}} + \sqrt{(\Delta_1 + \Delta_{\bar{1}})^2 - 4\Delta_c^2}), \quad (44)$$

$$\xi_3 = \hbar v_F / \Delta_{\bar{1}}, \quad (45)$$

are inversely proportional to the gaps in the spectrum opened at the Fermi points $\pm k_F$.⁷⁷

C. Kramers Pairs of Parafermions in Fractional Topological Insulators

After having considered the non-interacting model, we focus now on the fractional topological insulators that, again, find their origin in strong electron-electron interactions.⁷⁴ Similarly to the previous section, the elementary excitations carry the fractional charge e/m , with m a positive odd integer. Again, the fermionic operators R_τ and L_τ are redefined in terms of chiral bosonic fields $\phi_{r\tau}$, $R_\tau = e^{im\phi_{1\tau}}$ and $L_\tau = e^{im\phi_{\bar{1}\tau}}$. By analogy, in Nambu representation, we also introduce chiral bosonic operators $\phi_{1\tau}$ for holes. The commutation relations be-

tween fields are chosen to be

$$[\phi_{r\tau}(x), \phi_{r\tau}(x')] = \frac{i\pi r\tau}{m} \text{sgn}(x - x'), \quad (46)$$

$$[\tilde{\phi}_{r\tau}(x), \tilde{\phi}_{r\tau}(x')] = \frac{i\pi r\tau}{m} \text{sgn}(x - x'), \quad (47)$$

$$[\phi_{11}, \phi_{\bar{1}\bar{1}}] = [\phi_{11}, \tilde{\phi}_{\bar{1}\bar{1}}] = [\phi_{\bar{1}\bar{1}}, \tilde{\phi}_{11}] = \frac{i\pi}{m}, \quad (48)$$

$$[\tilde{\phi}_{\bar{1}\bar{1}}, \phi_{11}] = [\tilde{\phi}_{11}, \phi_{11}] = [\tilde{\phi}_{\bar{1}\bar{1}}, \tilde{\phi}_{11}] = \frac{i\pi}{m}, \quad (49)$$

$$[\phi_{\bar{1}\bar{1}}, \phi_{1\bar{1}}] = [\phi_{\bar{1}\bar{1}}, \tilde{\phi}_{11}] = [\phi_{1\bar{1}}, \tilde{\phi}_{\bar{1}\bar{1}}] = -\frac{i\pi}{m}, \quad (50)$$

$$[\tilde{\phi}_{\bar{1}\bar{1}}, \phi_{\bar{1}\bar{1}}] = [\tilde{\phi}_{\bar{1}\bar{1}}, \phi_{1\bar{1}}] = [\tilde{\phi}_{1\bar{1}}, \tilde{\phi}_{11}] = -\frac{i\pi}{m}, \quad (51)$$

where $r = \pm 1$. This choice is made under the constraint that all operators considered in this section that commute with each other in the fermionic representation do also commute in the bosonic representation. In particular, we pay attention to the fact that H_c and H_τ do not commute with each other whereas H_1 commutes with $H_{\bar{1}}$. These observations can be easily checked in the fermionic language [see Eqs. (36) and (37)].

Bosonizing H_τ and H_c , we arrive at

$$H_1 = \Delta_1 (\cos[m(\phi_{11} - \tilde{\phi}_{\bar{1}\bar{1}})] - \cos[m(\tilde{\phi}_{11} - \phi_{\bar{1}\bar{1}})]), \quad (52)$$

$$H_{\bar{1}} = \Delta_{\bar{1}} (\cos[m(\tilde{\phi}_{\bar{1}\bar{1}} - \phi_{\bar{1}\bar{1}})] - \cos[m(\phi_{1\bar{1}} - \tilde{\phi}_{\bar{1}\bar{1}})]), \quad (53)$$

$$H_c = \Delta_c (\cos[m(\phi_{11} - \tilde{\phi}_{\bar{1}\bar{1}})] + \cos[m(\tilde{\phi}_{11} - \phi_{\bar{1}\bar{1}})] - \cos[m(\tilde{\phi}_{11} - \phi_{1\bar{1}})] - \cos[m(\phi_{1\bar{1}} - \tilde{\phi}_{\bar{1}\bar{1}})]). \quad (54)$$

As already noted in Sec. II, if two operators, for example H_c and H_τ , do not commute with each other, they cannot be ordered simultaneously in the strong coupling regime. Thus, only the coupling constant corresponding to the most relevant term scales up. The competing term scales down and becomes irrelevant.

Further we consider the regime where crossed Andreev pairing dominates in one region ($0 < x < L$) while the usual pairing dominates in the two neighboring regions ($x < 0$ and $x > L$). Thus, we obtain the desired interfaces between two non-commuting terms. In addition, we again divide the total Hamiltonian into two parts $H^{(1)}$ and $H^{(\bar{1})}$ that act in two time-reversal symmetry conjugated subspaces: $(\phi_{11}, \phi_{\bar{1}\bar{1}}, \tilde{\phi}_{11}, \tilde{\phi}_{\bar{1}\bar{1}})$ and $(\phi_{\bar{1}\bar{1}}, \phi_{1\bar{1}}, \tilde{\phi}_{11}, \tilde{\phi}_{\bar{1}\bar{1}})$. From now on, we focus only on $H^{(1)}$ and rewrite it in terms of new bosonic fields ϕ_η and θ_η with $\eta = \pm 1$,

$$\phi_{rr} = \left[\frac{(\phi_1 + \theta_1)}{m} + r\phi_{\bar{1}} + r\theta_{\bar{1}} \right] / 2, \quad (55)$$

$$\tilde{\phi}_{r\bar{r}} = \left[\frac{(-\phi_1 + \theta_1)}{m} + r\phi_{\bar{1}} - r\theta_{\bar{1}} \right] / 2. \quad (56)$$

As a result, we arrive at

$$H_1^{(1)} = \Delta_1 \cos[\phi_1 + m\phi_{\bar{1}}], \quad (57)$$

$$H_{\bar{1}}^{(1)} = \Delta_{\bar{1}} \cos[\phi_1 - m\phi_{\bar{1}}], \quad (58)$$

$$H_c^{(1)} = \Delta_c (\cos[\phi_1 + m\theta_{\bar{1}}] + \cos[\phi_1 - m\theta_{\bar{1}}]) = 2\Delta_c \cos(\phi_1) \cos(m\theta_{\bar{1}}). \quad (59)$$

The commutation relations between the new ϕ - θ fields follow from Eqs. (46)-(51),

$$[\phi_{\bar{1}}(x), \theta_{\bar{1}}(x')] = \frac{2i\pi}{m} \theta(x - x'), \quad (60)$$

$$[\phi_1, \phi_{\bar{1}}] = [\phi_1, \theta_{\bar{1}}] = 0. \quad (61)$$

In addition, each field commutes with itself.

To minimize the total energy in the strong coupling regime, the fields standing under the cosines in $H_\tau^{(1)}$ and $H_c^{(1)}$ should be uniformly pinned in the corresponding regions where these terms are dominant.^{35,37} Consequently, the bulk energy spectrum is fully gapped, and the size of the gap is determined by the renormalized value of Δ_c (Δ_1 and $\Delta_{\bar{1}}$) at $0 < x < L$ ($x < 0$ and $x > L$). The field ϕ_1 is pinned uniformly, $\phi_1 = \pi\hat{M}$. The two other fields are pinned inside the corresponding regions,

$$\phi_{\bar{1}} = \begin{cases} \pi(\hat{M} + 1 + 2\hat{l}_{\bar{1}})/m, & x < 0 \\ \pi(\hat{M} + 1 + 2\hat{l}_1)/m, & x > L \end{cases}, \quad (62)$$

$$\theta_{\bar{1}} = \pi(\hat{M} + 1 + 2\hat{n})/m, \quad 0 < x < L. \quad (63)$$

Here, \hat{M} , $\hat{l}_{\pm 1}$, and \hat{n} are integer valued operators. The only non-zero commutation relation is between \hat{l}_1 and \hat{n} ,

$$[\hat{l}_1, \hat{n}] = \frac{im}{2\pi}. \quad (64)$$

Next, we can define two operators $\alpha_{\bar{1}}$ acting at $x = 0$ and α_1 acting at $x = L$,

$$\alpha_{\bar{1}} = e^{i\frac{2\pi}{m}(\hat{l}_{\bar{1}} + \hat{n})}, \quad \alpha_1 = -e^{i\frac{2\pi}{m}(\hat{l}_1 + \hat{n})}. \quad (65)$$

These two α operators commute with the Hamiltonian and thus correspond to zero-energy states.³⁵ In addition, they satisfy the commutation relations for \mathbb{Z}_m parafermions,

$$\alpha_1^m = 1, \quad \alpha_{\bar{1}}^m = 1, \quad \alpha_1 \alpha_{\bar{1}} = \alpha_{\bar{1}} \alpha_1 e^{-2\pi i/m}. \quad (66)$$

To conclude, similarly to the previous section, we identify the ground state degeneracy explicitly. We note that $(\alpha_1^\dagger \alpha_{\bar{1}})^m = 1$. Thus, the operator $\alpha_1^\dagger \alpha_{\bar{1}}$ has m eigenvalues $e^{2\pi i q/m}$ with $q = 0, \dots, m-1 \pmod{m}$ corresponding to the eigenstates $|q\rangle$. This confirms that the ground state of $H_1^{(1)}$ is m -fold degenerate,^{35,37} whereas the ground state of the total time-reversal invariant Hamiltonian $H = H_1^{(1)} + H_{\bar{1}}^{(1)}$ consists of m Kramers pairs of localized states.

IV. CONCLUSIONS

We propose two setups in which we generate Kramers partners of Majorana fermions and parafermions. Each setup is based on two topological insulators coupled via proximity to an s -wave superconductor. The mutual propagation directions of edge modes is different in the

two setups. In the para-helical (ortho-helical) setup, each of the two spin-up modes are moving in the same direction (in opposite directions) along their common edge. Such setups can be realized either by placing two topological insulators with the same spin orbit interaction sign next to each other (ortho-helical setup) or by placing them on top of each other (para-helical setup). In addition, the chemical potentials should be adjusted in such a way that crossed Andreev pairing via the s -wave superconductor is made possible. Moreover, this particular pairing, which is non-local, dominates over the usual one in the regime of strong electron-electron interactions. Taking into account that our scheme relies crucially on crossed Andreev pairing which has not been demonstrated yet in experiments with topological insulators (but was successfully implemented in experiments on Cooper pair splitters^{69,70}), we hope that such tests will be performed in the near future. For examples, signatures of such a pairing can be seen in noise measurements.⁷¹ Overall, taking into account that the coupling between topological insulators and superconductors was successfully implemented,⁶⁴ we believe that inducing both usual and crossed Andreev pairings is challenging but can be expected to be within experimental reach.

Zero-energy bound states arise at interfaces between two regions: in one of them the dominant pairing is the

crossed Andreev coupling, while in the other the usual one. As a result, such an interface hosts a Kramers pair of parafermions if the topological insulator supports fractional edge states. Otherwise, it hosts a Kramers pair of Majorana fermions.

Interfaces between regions can be shifted by local gates as it was first proposed for nanowires hosting Majorana fermions.²⁷ This allows us to envisage networks based on topological insulator edge modes that can serve as a platform for topological quantum computation. Moreover, the fact that we do not invoke any magnetic fields, which would be detrimental for superconductivity and the topological protection of the edge states in the topological insulators, helps us to extend our setup to a sea of parafermions that could host excitations obeying the Fibonacci type braiding statistics.^{37,40}

ACKNOWLEDGMENTS

We thank the UCSB KITP for hospitality where part of this work was performed. JK acknowledges funding from the Harvard Quantum Optics Center; AY from the NSF through grant DMR-1206016; a grant from Microsoft Corporation; and the STC Center for Integrated Quantum Materials, NSF grant DMR-1231319; and DL from the Swiss NSF and the NCCR QSIT.

-
- ¹ N. Read and D. Green, Phys. Rev. B **61**, 10267 (2000).
² L. Fu and C. L. Kane, Phys. Rev. Lett. **100**, 096407 (2008).
³ Y. Tanaka, T. Yokoyama, and N. Nagaosa, Phys. Rev. Lett. **103**, 107002 (2009).
⁴ M. Sato and S. Fujimoto, Phys. Rev. B **79**, 094504 (2009).
⁵ R. M. Lutchyn, J. D. Sau, and S. Das Sarma, Phys. Rev. Lett. **105**, 077001 (2010).
⁶ Y. Oreg, G. Refael, and F. von Oppen, Phys. Rev. Lett. **105**, 177002 (2010).
⁷ J. Alicea, Phys. Rev. B **81**, 125318 (2010).
⁸ L. Jiang, T. Kitagawa, J. Alicea, A. Akhmerov, D. Pekker, G. Refael, J. I. Cirac, E. Demler, M. D. Lukin, and P. Zoller, Phys. Rev. Lett. **106**, 220402 (2011).
⁹ S. Gangadharaiah, B. Braunecker, P. Simon, and D. Loss, Phys. Rev. Lett. **107**, 036801 (2011).
¹⁰ A. C. Potter and P. A. Lee, Phys. Rev. B **83**, 094525 (2011).
¹¹ J. Klinovaja, S. Gangadharaiah, and D. Loss, Phys. Rev. Lett. **108**, 196804 (2012).
¹² J. Klinovaja, G. J. Ferreira, and D. Loss, Phys. Rev. B **86**, 235416 (2012).
¹³ J. Klinovaja, P. Stano, and D. Loss, Phys. Rev. Lett. **109**, 236801 (2012).
¹⁴ J. Klinovaja, P. Stano, A. Yazdani, and D. Loss, Phys. Rev. Lett. **111**, 186805 (2013).
¹⁵ B. Braunecker and P. Simon, Phys. Rev. Lett. **111**, 147202 (2013).
¹⁶ M. Vazifeh and M. Franz, Phys. Rev. Lett. **111**, 206802 (2013).
¹⁷ J. Klinovaja and D. Loss, Phys. Rev. X **3**, 011008 (2013).
¹⁸ C. Dutreix, M. Guigou, D. Chevallier, and C. Bena, arXiv:1309.1143.
¹⁹ J. Klinovaja and D. Loss, Phys. Rev. B **88**, 075404 (2013).
²⁰ S. Sasaki, M. Kriener, K. Segawa, K. Yada, Y. Tanaka, M. Sato, and Y. Ando, Phys. Rev. Lett. **107**, 217001 (2011).
²¹ V. Mourik, K. Zuo, S. M. Frolov, S. R. Plissard, E. P. A. M. Bakkers, and L. P. Kouwenhoven, Science, **336**, 1003 (2012).
²² M. T. Deng, C. L. Yu, G. Y. Huang, M. Larsson, P. Caroff, and H. Q. Xu, Nano Lett. **12**, 6414 (2012).
²³ A. Das, Y. Ronen, Y. Most, Y. Oreg, M. Heiblum, and H. Shtrikman, Nat. Phys. **8**, 887 (2012).
²⁴ L. P. Rokhinson, X. Liu, and J. K. Furdyna, Nat. Phys. **8**, 795 (2012).
²⁵ J. R. Williams, A. J. Bestwick, P. Gallagher, S. S. Hong, Y. Cui, A. S. Bleich, J. G. Analytis, I. R. Fisher, and D. Goldhaber-Gordon, Phys. Rev. Lett. **109**, 056803 (2012).
²⁶ H. O. H. Churchill, V. Fatemi, K. Grove-Rasmussen, M. Deng, P. Caroff, H. Q. Xu, and C. M. Marcus, Phys. Rev. B **87**, 241401(R) (2013).
²⁷ J. Alicea, Y. Oreg, G. Refael, F. von Oppen, and M. P. A. Fisher, Nat. Phys. **7**, 412 (2011).
²⁸ J. K. Pachos, *Introduction to Topological Quantum Computation*, Cambridge University Press (2012).
²⁹ E. Fradkin and L. P. Kadanoff, Nucl. Phys. B **170**, 1 (1980).
³⁰ M. Barkeshli and X.-L. Qi, Phys. Rev. X **2**, 031013 (2012).
³¹ P. Fendley, J. Stat. Mech. **2012**, 11020 (2012).
³² M. Cheng, Phys. Rev. B **86**, 195126 (2012).

- ³³ N. Lindner, E. Berg, G. Refael, and A. Stern, *Phys. Rev. X* **2**, 041002 (2012).
- ³⁴ A. Vaezi, *Phys. Rev. B* **87**, 035132 (2013).
- ³⁵ D. Clarke, J. Alicea, and K. Shtengel, *Nat. Commun.* **4**, 1348 (2013).
- ³⁶ Y. Oreg, E. Sela, and A. Stern, arXiv:1301.7335.
- ³⁷ R. Mong, D. Clarke, J. Alicea, N. Lindner, P. Fendley, C. Nayak, Y. Oreg, A. Stern, E. Berg, K. Shtengel, and M. P. A. Fisher, arXiv:1307.4403.
- ³⁸ A. Vaezi, arXiv:1307.8069.
- ³⁹ J. Klinovaja and D. Loss, arXiv:1311.3259.
- ⁴⁰ J. Klinovaja and D. Loss, arXiv:1312.1998.
- ⁴¹ C. L. M. Wong and K. T. Law, *Phys. Rev. B* **86**, 184516 (2012).
- ⁴² S. B. Chung, J. Horowitz, and X.-L. Qi, arXiv:1208.3928.
- ⁴³ F. Zhang, C. L. Kane, and E. J. Mele, *Phys. Rev. Lett.* **111**, 056402 (2013).
- ⁴⁴ S. Nakosai, J. K. Budich, Y. Tanaka, B. Trauzettel, and N. Nagaosa, *Phys. Rev. Lett.* **110**, 117002 (2013).
- ⁴⁵ S. Deng, L. Viola, and G. Ortiz, *Phys. Rev. Lett.* **108**, 036803 (2012).
- ⁴⁶ A. Keselman, L. Fu, A. Stern, and E. Berg, *Phys. Rev. Lett.* **111**, 116402 (2013).
- ⁴⁷ X.-J. Liu, C. L. M. Wong, and K. T. Law, arXiv:1304.3765.
- ⁴⁸ E. Gaidamauskas, J. Paaske, and K. Flensberg, arXiv:1309.2808.
- ⁴⁹ E. Dumitrescu, J. Sau, and S. Tewari, arXiv:1310.7938.
- ⁵⁰ A. Haim, A. Keselman, E. Berg, and Y. Oreg, arXiv:1310.4525.
- ⁵¹ M.Z. Hasan and C.L. Kane, *Rev. Mod. Phys.* **82**, 3045 (2010).
- ⁵² B.A. Volkov and O.A. Pankratov, *JETP Lett.* **42**, 178 (1985).
- ⁵³ O.A. Pankratov, S.V. Pakhomov, and B.A. Volkov, *Solid State Commun.* **61**, 93 (1987).
- ⁵⁴ O.A. Pankratov and B.A. Volkov, in *Landau Level Spectroscopy*, edited by E.I. Rashba and G. Landwehr (North-Holland, Amsterdam, 1991), Chap. 14, p. 817.
- ⁵⁵ L. Fu, C.L. Kane, and E.J. Mele, *Phys. Rev. Lett.* **98**, 106803 (2007).
- ⁵⁶ X.-L. Qi, T.L. Hughes, and S.-C. Zhang, *Phys. Rev. B* **78**, 195424 (2008).
- ⁵⁷ P. Michetti, J. C. Budich, E. G. Novik, and P. Recher, *Phys. Rev. B* **85**, 125309 (2012).
- ⁵⁸ S. I. Erlingsson and J. C. Egues, arXiv:1312.2034
- ⁵⁹ M. König, S. Wiedmann, C. Brune, A. Roth, H. Buhmann, L. W. Molenkamp, X. Qi, and S. Zhang, *Science* **318**, 766 (2007).
- ⁶⁰ M. König, H. Buhmann, L. W. Molenkamp, T. Hughes, C. Liu, X. Qi, and S. Zhang, *J. Phys. Soc. Jpn.* **77**, 031007 (2008).
- ⁶¹ A. Roth, C. Brune, H. Buhmann, L. W. Molenkamp, J. Maciejko, X. Qi, and S. Zhang, *Science* **325**, 294 (2009).
- ⁶² J. Wang, H. Li, C. Chang, K. He, J. Lee, H. Lu, Y. Sun, X. Ma, N. Samarth, S. Shen, Q. Xue, M. Xie, and M. Chan, *Nano Res.* **5**, 739 (2012).
- ⁶³ K. C. Nowack, E. M. Spanton, M. Baenninger, M. König, J. R. Kirtley, B. Kalisky, C. Ames, P. Leubner, C. Brune, H. Buhmann, L. W. Molenkamp, D. Goldhaber-Gordon, and K. A. Moler, arXiv:1212.2203.
- ⁶⁴ S. Hart, H. Ren, T. Wagner, P. Leubner, M. Mühlbauer, C. Brune, H. Buhmann, L. W. Molenkamp, and A. Yacoby, arXiv:1312.2559.
- ⁶⁵ G. Deutscher and D. Feinberg, *Appl. Phys. Lett.* **76**, 487 (2000).
- ⁶⁶ P. Recher, E. V. Sukhorukov, and D. Loss, *Phys. Rev. B* **63**, 165314 (2001).
- ⁶⁷ P. Recher and D. Loss, *Phys. Rev. B* **65**, 165327 (2002).
- ⁶⁸ C. Bena, S. Vishveshwara, L. Balents, and M. P. A. Fisher, *Phys. Rev. Lett.* **89**, 037901 (2002).
- ⁶⁹ L. Hofstetter, S. Csonka, J. Nygard, and C. Schonenberger, *Nat.* **461**, 960 (2009).
- ⁷⁰ A. Das, Y. Ronen, M. Heiblum, D. Mahalu, A. Kretinin, and H. Shtrikman, *Nat. Commun.* **3**, 1165 (2012).
- ⁷¹ K. Sato, D. Loss, and Y. Tserkovnyak, *Phys. Rev. Lett.* **105**, 226401 (2010).
- ⁷² K. Sato, D. Loss, and Y. Tserkovnyak, *Phys. Rev. B* **85**, 235433 (2012).
- ⁷³ R. Reinthaler, P. Recher, and E. Hankiewicz, *Phys. Rev. Lett.* **110**, 226802 (2013).
- ⁷⁴ M. Levin and A. Stern, *Phys. Rev. Lett.* **103**, 196803 (2009).
- ⁷⁵ A.A. Zyuzin, D. Rainis, J. Klinovaja, and D. Loss, *Phys. Rev. Lett.* **111**, 056802 (2013).
- ⁷⁶ B. Braunecker, G. I. Japaridze, J. Klinovaja, and D. Loss, *Phys. Rev. B* **82**, 045127 (2010).
- ⁷⁷ J. Klinovaja and D. Loss, *Phys. Rev. B* **86**, 085408 (2012).
- ⁷⁸ J. Klinovaja and D. Loss, *Phys. Rev. Lett.* **110**, 126402 (2013).
- ⁷⁹ D. Rainis, L. Trifunovic, J. Klinovaja, and D. Loss, *Phys. Rev. B* **87**, 024515 (2013).
- ⁸⁰ In spite of the fact that fractional excitations with fractional charge, such as $e/3$, can be constructed explicitly if backscattering terms are taken into account,^{81–84} we follow here the approach of Ref. 74 that postulates appropriate commutation relations for fractional topological insulator excitations.
- ⁸¹ C. L. Kane, R. Mukhopadhyay, and T. C. Lubensky, *Phys. Rev. Lett.* **88**, 036401 (2001).
- ⁸² J. C. Y. Teo and C. L. Kane, arXiv:1111.2617.
- ⁸³ J. Klinovaja and D. Loss, *Phys. Rev. Lett.* **111**, 196401 (2013).
- ⁸⁴ J. Klinovaja and D. Loss, arXiv:1305.1569.
- ⁸⁵ T. Giamarchi, *Quantum Physics in One Dimension* (Oxford University Press, Oxford, 2004).